Asymmetry in Three-Site Relaxation-Exchange NMR

Bernhard Blümich,[1] Matthew Parziale,[2] and Matthew Augustine[2]

[1] Institut für Technische und Makromolekulare Chemie, RWTH Aachen University, Worringer Weg 2, 52074 Aachen, Germany

[2] Department of Chemistry, UC Davis, One Shields Avenue, Davis, CA 95616, USA

Corresponding author: Bernhard Blümich, bluemich@itmc.rwth-aachen.de

Asymmetry of peak integrals in 2D relaxation maps of exchange between three sites reports circular flow between the relaxation sites. This disagrees with detailed balance according to which the exchange between any pair of sites must be balanced in thermodynamic equilibrium. Confined diffusion of particles jumping randomly on a 2D checkerboard grid to any of their eight neighbor positions and confined gas diffusion were modelled in Monte Carlo simulations to explore the impact of topological constraints on particle exchange between three pools. Both models produce density variations across the pore and reveal that up to 1% of the molecules move in circular paths between the relaxation pools. This motion is driven by different features of either algorithm. It is silent in thermodynamic equilibrium, confirming that multisite exchange maps are symmetric in this case. The coherent flux is argued to result from stochastic pore resonance related to diffusion eigenmodes. If it can be driven experimentally by external time-varying electric, magnetic or ultrasonic fields, this may be a way to enhance heterogeneous catalysis.

1. Introduction

Exchange is an essential ingredient of diffusion and spreading phenomena, which are abundant in nature and govern the evolution of tangible and intangible objects and goods (Bunde et al., 2018) as well as the physics of living systems (Gnesotto et al., 2018; Lynn et al., 2021). Nuclear Magnetic Resonance provides particularly powerful methodologies to investigate molecular exchange processes (Ernst et al., 1987; Callaghan, 2011). Slow molecular exchange on the millisecond time scale is studied by e. g. two-dimensional exchange NMR, i. e. by chemical exchange spectroscopy for rotational motion (Jeener et al., 1979) and by exchange relaxometry for translational motion (Lee et al., 1993). In equilibrium the nature of the exchange processes is commonly understood to be random Brownian motion, and the associated 2D NMR exchange maps are expected to be symmetric with respect to their diagonal. On the other hand, exchange in non-equilibrium leads to asymmetry. This has been observed in NMR, for example, in 2D chemical exchange spectra for chemical reactions involving different sites (Lacabanne et al., 2022), for the spread of hyperpolarization by spin diffusion (Björgvinsdóttir et al., 2021), for slow flow across porous media in relaxation exchange maps (Olaru et al., 2012), as well as in position- and velocity-exchange NMR (Han and Blümich, 2000).

The kinetics of transitions or exchange between discrete states driven by random processes are described by (van Kampen, 1992)

$$\frac{\mathrm{d}M_i(t)}{\mathrm{d}t} = \sum_j \left\{ k_{ij} M_j(t) - k_{ji} M_i(t) \right\}, \tag{1}$$

where M_i are populations represented in NMR by magnetization components collected in the vector $\boldsymbol{M}$, and k_{ij} are the exchange rates equivalent to the transition probabilities from state *j* to state *i*, which are collected in the kinetic exchange matrix $\mathbf{k}$. In equilibrium

$$\frac{\mathrm{d}M_i(t)}{\mathrm{d}t} = 0, \tag{2}$$

and the number of all particles arriving at site *i* from sites *j* is equal to the number of all particles leaving from site *i* to sites *j* so that the total mass is conserved.

As a result of mass balance, two-site exchange between states or sites A and B always leads to symmetric 2D NMR exchange maps in thermodynamic equilibrium as the number $k_{\mathrm{BA}} M_{\mathrm{A}}$ of particles populating site B by leaving site A per unit time is equal to the number of particles $k_{\mathrm{AB}} M_{\mathrm{B}}$ leaving site B and populating site A per unit of time. This number is the product of the rate k_{BA} for transitions from site A to site B

times the population M_{A} of site A. The relationship $k_{\mathrm{BA}}M_{\mathrm{A}} = k_{\mathrm{AB}}M_{\mathrm{B}}$ is known as the 'principle of detailed balance'. In thermal equilibrium it is understood to also apply to rate processes involving more than two sites (Onsager 1931, Gnesotto et. al. 2018).

By example of mass-balanced equilibrium diffusion between three sites (Onsager 1931, Sandstrom, 1983), Eqn. (1) becomes

$$\begin{aligned} k_{21}M_1 + k_{31}M_1 &= k_{12}M_2 + k_{13}M_3, \\ k_{12}M_2 + k_{32}M_2 &= k_{21}M_1 + k_{23}M_3, \\ k_{13}M_3 + k_{23}M_3 &= k_{31}M_1 + k_{32}M_2, \end{aligned} \tag{3}$$

or equivalently, mass balance requires

$$k_{31}M_1 - k_{13}M_3 = k_{12}M_2 - k_{21}M_1 = k_{23}M_3 - k_{32}M_2. \tag{4}$$

Normalization of this expression to the total number of exchanges per unit time defines the asymmetry parameter a_{sy} used below,

$$(k_{23}M_3 - k_{32}M_2)/[(1,1,1)\,\mathbf{k}\,\boldsymbol{M}] \stackrel{\text{def}}{=} a_{\mathrm{sy}}. \tag{5}$$

Here $k_{ij}M_j$ is the number of transitions from pool j to pool i, corresponding to the peak integral in an exchange map after correction for relaxation effects, so that the denominator corresponds to the integral over all peaks. The asymmetry parameter thus quantifies the imbalance of exchange between two sites in terms of the number of unbalanced exchanges normalized to the total number of exchanges. Therefore, it specifies the relative flux in the circular exchange process. While mass balance (4) is a necessary condition for dynamic equilibrium, detailed balance, on the other hand, is a stronger condition applicable to thermodynamic equilibrium. It requires

$$a_{\mathrm{sy}} = 0. \tag{6}$$

Detailed balance had been introduced by Maxwell in 1867 based on 'sufficient reason' in his derivation of the speed distribution of gas atoms considering the speed exchange between colliding gas atoms in thermodynamic equilibrium (Maxwell, 1867). An intriguing consequence of the exchange being balanced in detail between particles A and B amounts to the impossibility of assigning positive time to either velocity exchange from A to B or B to A on the particle scale of the exchange process, thus admitting negative time or time reversal. In 1872 Boltzmann showed in an elaborate treatment, that Maxwell's speed distribution also applies to polyatomic gas molecules (Boltzmann, 1872). Furthermore, in 1917 Einstein derived Planck's law of black-body radiation as a balanced energy exchange between quantized radiation and matter underlining the striking similarity to Maxwell's speed distribution of gas atoms (Einstein, 1917). He concludes "Indem Energie und Impuls aufs engste miteinander verknüpft

sind, kann deshalb eine Theorie erst dann als berechtigt angesehen werden, wenn gezeigt ist, daß die nach ihr von der Strahlung auf die Materie übertragenen Impulse zu solchen Bewegungen führen, wie sie die Wärmetheorie verlangt," (Since energy and momentum are intimately connected, a theory can only then be considered justified, when it has been shown, that according to it the momenta of the radiation transferred to the matter lead to such motions as demanded by the theory of heat.)

In his work extending Maxwell's speed distribution to polyatomic gas molecules Boltzmann considered molecules in a container whereby the walls reflect the molecules like elastic balls: "Bezüglich der Gefäßwände, welche das Gas umschließen, will ich jedoch voraussetzen, dass die Moleküle an denselben wie elastische Kugeln reflektiert werden. … Die Wände stören nicht, da an ihnen die Moleküle wie elastische Kugeln reflektiert werden; also geradeso von ihnen zurücktreten, als ob der Raum jenseits der Wände von gleich beschaffenem Gase erfüllt wäre." (Concerning the container walls which enclose the gas, I want to presume that the molecules are reflected from them like elastic balls. …. The walls do not interfere, because the molecules are reflected from them like elastic balls; that is, recede from them just like that, as if the space beyond the walls would be filled with similarly conditioned gas.) Moreover, the interaction between gas molecules can be of any type. While Boltzmann states that any other interaction between walls and molecules leads to the same result albeit at loss of simplicity, the perfectly elastic reflections of the gas molecules at the walls eliminate the topological constraints of the box on their motion. For confined particles, this means that the pressure across the pore volume is constant, i. e. the time average of the particle density does not vary with the location inside the pore. Boltzmann obtained the same speed distribution for polyatomic molecules with internal degrees of freedom as Maxwell had for atoms based on detailed balance of speed exchange. In the simulations reported below, the motion of molecules is considered for which the interactions with the walls are the same as those among the molecules. Understanding confined diffusion (Valiullin, 2017) is important from a general point of view because the motion of molecules without topological constraints is an ideal limit which cannot perfectly be realized in practice although it may be realized within experimental uncertainty.

Two-site exchange processes will always be symmetric in equilibrium. This situation has been evaluated analytically for NMR relaxation exchange of fluids in porous media (McDonald, 2005). Yet multi-site relaxation-exchange NMR maps (Van

Landeghem, 2010) can formally be asymmetric in equilibrium. For example, the transverse magnetization $s(t_1, t_2)$ from a three-site T_2-T_2 relaxation exchange NMR experiment (Gao and Blümich, 2020),

$$s(t_1, t_2) = (1,1,1)e^{-(\mathbf{R}_2+\mathbf{k})t_2}e^{-(\mathbf{R}_1+\mathbf{k})t_\mathrm{m}}e^{-(\mathbf{R}_2+\mathbf{k})t_1}\boldsymbol{M}(t_0), \quad (7)$$

has been simulated to model an experimentally observed asymmetric three-site T_2-T_2 NMR exchange map of water molecules saturating Al_2O_3 powder with the three relaxation sites corresponding to bulk water, water molecules on the surface of the powder particles and water molecules inside the surface pores (Fig. 1). Here $\boldsymbol{M}(t_0)$ is the initial vector of transverse magnetization components from relaxation sites 1, 2 and 3 generated from longitudinal thermodynamic equilibrium magnetization with a 90° pulse at the beginning of the experiment at time t_0, and t_1, t_m, t_2 are the evolution, mixing, and detection time intervals of the 2D NMR experiment, respectively (Callaghan, 2011; Lee et al., 1993). Apart from the relaxation-rate matrices $\mathbf{R}_1$ and $\mathbf{R}_2$, and the kinetic matrix $\mathbf{k}$, the best match obtained by forward simulation returned the peak integrals revealing an asymmetry parameter of $a_\mathrm{sy} = -1.2\%$. This asymmetry of the forward and backward particle jumps between two sites specifies the relative circular flux between the three sites (Fig. 1).

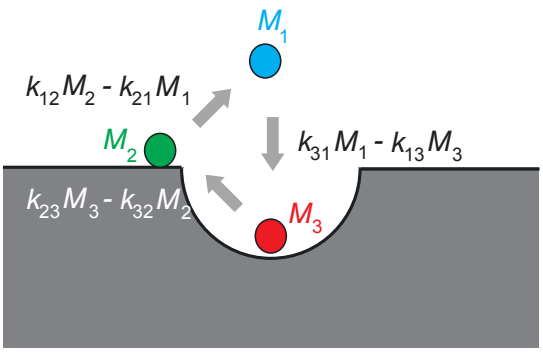

Figure 1. Asymmetry in three-site diffusion-mediated exchange indicates coherent circular motion in a model example of water molecules in contact with a porous surface. Three water populations M_j are identified by different NMR relaxation times and color. They are molecules in the bulk (1), molecules on the surface (2) and molecules in the pores (3). The exchange rate constants are k_{ji}. The net particle flux $k_{ij}M_j - k_{ji}M_i$ between two sites differs from zero. The net mass of all molecules participating in the exchange is conserved. The figure illustrates positive a_sy.

The asymmetry observed in the experiment can be argued to result from the uncertainty of the measurement and the data processing by 2D inverse Laplace transformation (Song 2002). Also, asymmetric three-site exchange disagrees with

detailed balance of the exchange between any pair of sites in thermodynamic equilibrium because it needs to be explained by circular diffusion on the pore scale, and such motion resembles that of a rachet which Feynman has argued to disagree with the second law of thermodynamics (Feynman et al., 1966). Nevertheless, Monte Carlo simulations were executed and are discussed below to investigate asymmetry in three-site exchange.

2. Modelling confined diffusion

2.1 Vacancy diffusion: Random particle jumps on a 2D checkerboard

Random jumps of particles from occupied sites to vacant sites were simulated with a Monte-Carlo algorithm (Metropolis et al., 1953; Grebenkov, 2011; Hughes, 1995; Sabelfeld, 1991) in a confined space on a checkerboard. The algorithm models vacancy diffusion (Seitz, 1948) encountered in metals and alloys but the particles perform the jumps rather than the vacancies. To keep the simulation simple, it is limited to jumps on a 2D 3×3 Moore lattice of range 1 (Wolf-Gladrow, 2000) following rules of the game of life (Wolf-Gladrow, 2000; Bialnicki-Birula, 2004). Here the center particle can jump to any of its 8 neighbors (Fig. 2). Different neighborhoods of range 1 were tested (Fig. S1) (Bialnicki-Birula, 2004), but only the Moore neighborhood having the highest symmetry of all neighborhoods, produced data consistent with Eqn. (4). Topological constraints are introduced which set boundaries to the jump space. Initially, the available cells inside the jump space on the grid are populated randomly with particles up to a specified particle density. Particles in the bulk are indexed 1, and two distinct boundary sections are indexed 2 and 3, giving three environments for the particles to be exposed to and between which randomly selected particles can move. A particle jumping from environment *j* to *i* is counted by incrementing the element *ij* of a 3×3 jump matrix with elements $k_{ij}M_j$ by 1. If the particle environment does not change with the jump, the respective diagonal element $k_{jj}M_j$ is incremented. The NMR relaxation environments are indexed according to increasing relaxation rate. If a particle is in contact with two different relaxation environments, it is assigned to the relaxation environment with the higher index according to the higher relaxation rate.

Different rules governing jumps to a neighbor cell were explored. 1) In the simplest case, one of the 8 destination cells was chosen at random without assigning a jump probability. When destination cell was free, the jump was executed, and the initial and final environments were compared to increment the corresponding entry in

the jump matrix accordingly. When the destination cell was occupied, the particle remained at its source cell, and the respective diagonal element of the jump matrix was incremented. In all other cases, jump probabilities were assigned. 2) As a subtle variant of the random jumps to any of the 8 neighbor cells, jumps were randomly selected to any of the *free* neighbor cells by assigning zero jump probability to occupied neighbor cells and equal probability for jumps to the empty cells. This algorithm is known to violate detailed balance (Metropolis et al., 1953; Reviewer, 2023). 3) With reference to the Helmholtz free energy $A = U - T\,S$, where U is internal energy, T is temperature, and S is entropy, a jump probability $p = \exp\left\{-\frac{\Delta A}{k_{\mathrm{B}}T}\right\}$ was introduced, where $\Delta A = \Delta U - T\,\Delta S$, T is the temperature, and k_{B} the Boltzmann constant. $\Delta U = -\boldsymbol{F}\,\Delta\boldsymbol{R}$ and ΔS were estimated from the sum of distances to free or occupied neighbor cells by crude empirical models as detailed in the supporting information. Here $\boldsymbol{F}$ is the force and $\Delta\boldsymbol{R}$ the distance vector between two particles. This allowed probing attractive and repulsive interactions by changing the sign of ΔU in simulation runs and varying temperature in addition to varying population density equivalent to pressure. It is noted here that the force field on a randomly populated lattice is not conservative (Reviewer, 2023). In other words, the energy balance of a particle moving in a circle is different from zero, and Monte Carlo simulations under these constraints probe a driven equilibrium and not thermodynamic equilibrium (Michel et. al., 2014).

Figure 2. Jumps on a checkerboard grid modelling vacancy diffusion. The center particle can jump to any of its eight next nearest neighbor cells, which are numbered clockwise from 1 to 8. Jump probabilities were introduced to account for particle interaction between the center particle (red) and neighbor particles (black).

The vacancy-diffusion simulations were carried out with a program written in Matlab R2020a by The MathWorks Inc. on an Apple MacBook Pro 2.4 GHz having an Intel Quad-Core i5 processor. Unless indicated otherwise, 10^7 jumps were simulated in one run taking 75 seconds.

2.2 Gas diffusion

The gas diffusion calculations explore similar pore size and occupancy. Here the motion of circular particles with diameter equal to the cell size was accomplished by propagating an initial distribution of particle speeds for random initial positions and directions in a Monte Carlo fashion based on instantaneous collisional forces. This distribution rapidly equilibrated to a Maxwell-Boltzmann distribution. Whereas in vacancy-diffusion simulations the distribution of particles in the pore is recorded after each jump it is recorded in the gas-phase simulations at constant time intervals. If the center of each particle was within one diameter of another, the particles are considered to have collided. Immediately after a collision the projection of the velocity vector along the collision axis is reversed prior to propagating to the next step. In this approach, the observation time interval must be sufficiently small, so that the new velocities are calculated with a small position uncertainty of the colliding particles (Reviewer 2023, Michel et al. 2014).

The collisions change both the direction and velocity of the particles at each of the 10^9 constant time increments used here. Following conservation of momentum and kinetic energy,

$$\vec{v}_{1,\mathrm{new}} = \vec{v}_{1,\mathrm{old}} - \frac{2m_2}{(m_1+m_2)} \frac{\langle \vec{v}_{1,\mathrm{old}} - \vec{v}_{2,\mathrm{old}}, \vec{x}_1 - \vec{x}_2 \rangle}{\|\vec{x}_2 - \vec{x}_1\|^2} (\vec{x}_1 - \vec{x}_2), \tag{8}$$

$$\vec{v}_{2,\mathrm{new}} = \vec{v}_{2,\mathrm{old}} - \frac{2m_1}{(m_1+m_2)} \frac{\langle \vec{v}_{2,\mathrm{old}} - \vec{v}_{1,\mathrm{old}}, \vec{x}_2 - \vec{x}_1 \rangle}{\|\vec{x}_2 - \vec{x}_1\|^2} (\vec{x}_2 - \vec{x}_1). \tag{9}$$

These collisions with other particles and the wall are mediated by the particle size, which is set to be a fraction of the pore-side length of one. This means that a square pore with a five-particle diameter side length is populated with particles having a diameter of 1/5. To compare the continuous positional output of this model to vacancy diffusion, a two-dimensional square grid with cell size set by the particle diameter is imposed on the entire pore. The quasi-continuous positional output is then binned into these cells and compared to the binned positions from the previous observation to determine if particles translated between the main pore volume, pore wall, and active site. The translational information is used to assign estimates of the jump-matrix elements and thus the asymmetry parameter a_{sy}.

The gas-diffusion simulations were carried out with a program written in Matlab R2020a by The MathWorks Inc. on a home-built desktop computer possessing an AMD R y z e n 7 2 7 0 0 processor. In most cases, 10^9 jumps were simulated in one run taking roughly 45 hours to complete.

3. Results

Two different pore geometries were analyzed. Initially, the simulation was executed for a pore geometry (Fig. 3a) which approximates the surface structure of Fig. 1, and which is hypothesized to explain the observed asymmetry of water diffusing in a porous Al_2O_3 grain pack (Gao and Blümich, 2020). The dented surface was mirrored horizontally to double the probability of particles entering the dent (relaxation site 3) in the otherwise straight surface (relaxation site 2). The bulk of the particles defines relaxation site 1. Periodic boundary conditions were employed right and left. A pore boundary has been treated just like an occupied cell with the same rules applying to the jump probability. The simulations of particle motion confined to this complex pore structure and constrained by jump probabilities revealed the existence of asymmetric exchange. To understand the essence of the asymmetry the pore geometry was simplified to a square with an active site in the wall to study particle motion in detail. Particles in the bulk, in contact with the walls, and with the active site are identified by different NMR relaxation properties (Fig. 3b).

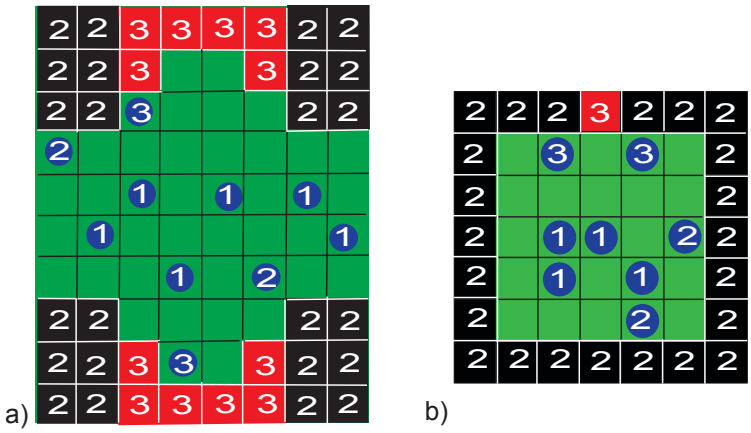

Figure 3. Examples of pore models for two-dimensional three-site exchange based on a checkerboard grid. Particles can occupy one cell and jump to a neighboring one following different realizations of the jump probability. a) Porous solid. The boundaries right and left are periodic. The boundaries top and bottom are rigid. Depending on their next neighbors in the first coordination shell, the particle-relaxation environments are identified as bulk (1), surface (2), and pore (3) with increasing relaxation rate. b) Small square pore with an active site. The bulk (1), the walls (2), and the active site (3) have different relaxation properties. If a particle is in contact with two different relaxation sites, it is counted to belong to the particle pool with the larger relaxation rate, i. e. the pool with the higher number.

Enabled by the interaction model, which, depending on the particle environment assigns different jump probabilities as a function of temperature, the asymmetry

parameter a_{sy} was evaluated for both pores with the vacancy-diffusion algorithm as a function of temperature T and pressure P. Pressure was varied in terms of the population density measured as the fraction of cells occupied in the pore. The results for the complex pore are reported in the supplementary material (Fig. S3), whereas those for the simple square pore are reported in the main text here (Fig. 4). At certain temperatures and pressures also the autocorrelation function of the occupation-time track of a particular cell and its Fourier transform were determined. Striking features observed in vacancy diffusion were subsequently modelled with the gas-diffusion algorithm in the square pore.

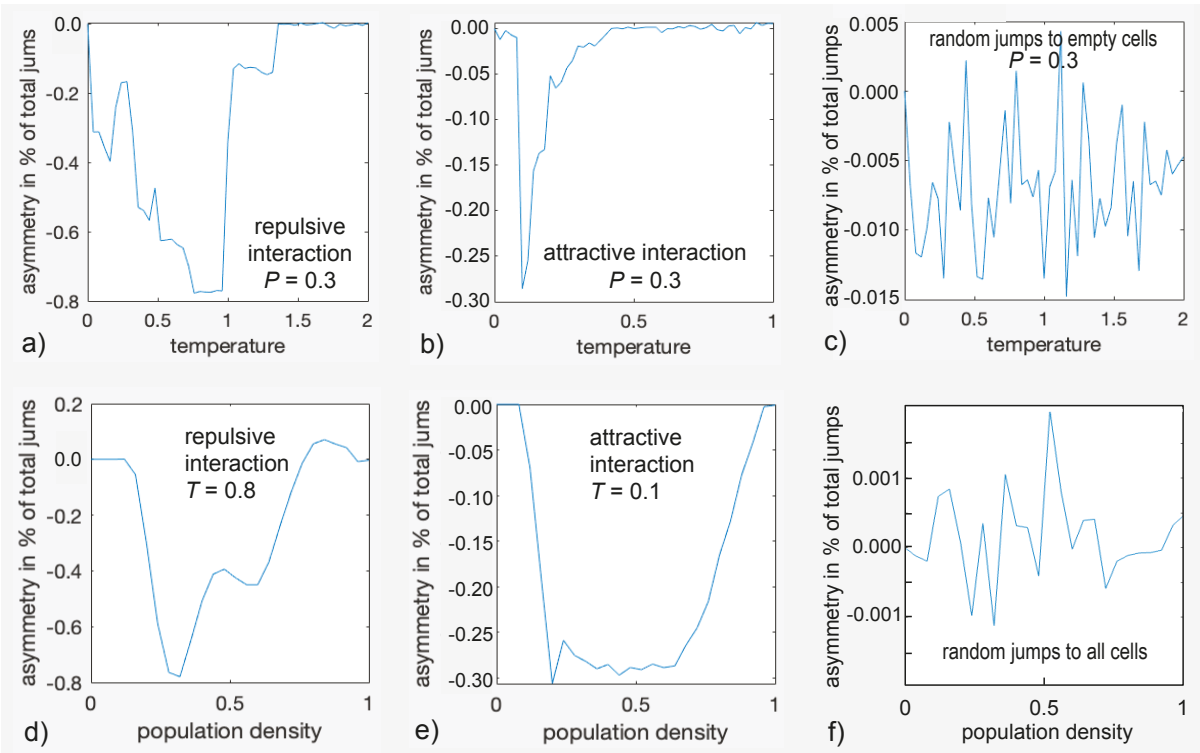

Figure 4. Asymmetry parameters a_{sy} for diffusion inside the small rectangular pore depicted in Fig. 3b as a function of temperature T (a-c) and pressure P (d-f). a) $a_{\mathrm{sy}}(T)$ for repulsive interaction at $P = 0.3$. b) $a_{\mathrm{sy}}(T)$ for attractive interaction at $P = 0.3$. c) $a_{\mathrm{sy}}(T)$ for jumps to randomly selected empty cells. d) $a_{\mathrm{sy}}(P)$ for attractive interaction at $T = 0.8$. e) $a_{\mathrm{sy}}(P)$ for attractive interaction at $T = 0.1$. f) $a_{\mathrm{sy}}(P)$ for jumps to cells randomly selected from all eight neighbor cells.

Relevant results for the square pore (Fig. 3b) are summarized in six graphs in Fig. 4. The asymmetry parameter varies strongly with temperature T (Figs. 4a,b) and pressure corresponding to population density P (Figs. 4d,e). All parameters are relative quantities without units. The top three graphs a), b) and c) show the variation of a_{sy} with temperature for a population fraction of 0.3 corresponding that of a gas. The

asymmetry parameter assumes only negative values in an abrupt but reproducible manner in the range of -0.8% < a_{sy} < 0.0% for repulsive interaction (Fig. 4a), i. e. for the definition of the force between particles as illustrated in Fig. S2a. With reference to Fig. 1, negative a_{sy} reports that the straight exit route from the active site towards the center of the pore is preferred over the detour via the pore wall. When the interaction is changed from repulsive to attractive by inverting the sign of ΔU in the expression for the free energy, the asymmetry parameter varies as well, however, only between -0.3% < a_{sy} < 0.0% (Fig. 4b). In either case, the asymmetry parameter varies with temperature and pressure. It is concluded, that for this small pore, up to about 1% of all jumps on the checkerboard can proceed in an ordered circular fashion between the three sites. Similar behavior is observed for the complex pore of Fig. 3a as illustrated in Fig. S3 in the supplement.

At the extrema of the $a_{\mathrm{sy}}(T)$ curves in Figs. 4a,b the dependence of the asymmetry parameters on population density was investigated (Figs. 4d,e). The variations with population density are smoother than those with temperature. Significant negative asymmetry results at intermediate pressure, while at low and high pressure, the asymmetry is small (Fig. 4d,e). At higher temperature and high pressure, small positive a_{sy} is observed (Fig. 4d, T = 0.8, P = 0.8). If the destination cell for a jump is chosen at random without considering a hypothetical free jump energy A, essentially noise more than two orders of magnitude smaller is observed for the exchange asymmetry determined from 10^7 jumps when varying T and P (Fig. 4c,f). However, a small bias towards negative a_{sy} results if the destination cell is chosen at random from all fee neighbor cells (Figs. 4c), whereas no bias is detected if the destination cell is chosen at random from all neighbor cells whether free or occupied (Fig. 4f). This difference becomes more pronounced at higher number of jumps (see below).

To shed further light on the origin of the asymmetry, autocorrelation functions of the occupation-time tracks of selected cells in the pore were computed and Fourier transformed (Fig. 5). The occupation-time track was calibrated to zero mean for purely random occupation, i. e. it contained the negative population density when it was empty and the complement of the population density to one when the cell was occupied. The faster the autocorrelation function decays, the less coherent the cell population fluctuates and the broader is its Fourier transform, i. e. the transfer function (Fig. 5b,c). A constant offset of the autocorrelation function shows that the time-average

population in the cell differs from the mean population of the pore (Fig. 5a,b). This offset produces a spike at zero frequency in the transfer functions. Subtracting the offsets from the autocorrelation functions and scaling the resulting functions to the same amplitude reveals different decays in different cells and thus variations in particle dynamics across the pore (inset in Fig. 5c, middle). These dynamics cannot readily be measured for a single cell in the pore, although an average over all cells and pores in the measurement volume would be amenable to experiment by probing the particle dynamics with CPMG measurements in magnetic gradient fields at variable echo time. Such measurements provide the frequency-dependent diffusion coefficient in terms of the Fourier transform of the velocity autocorrelation function (Stepišnik et al., 2014, Callaghan and Stepišnik, 1995; Parsons et al., 2006).

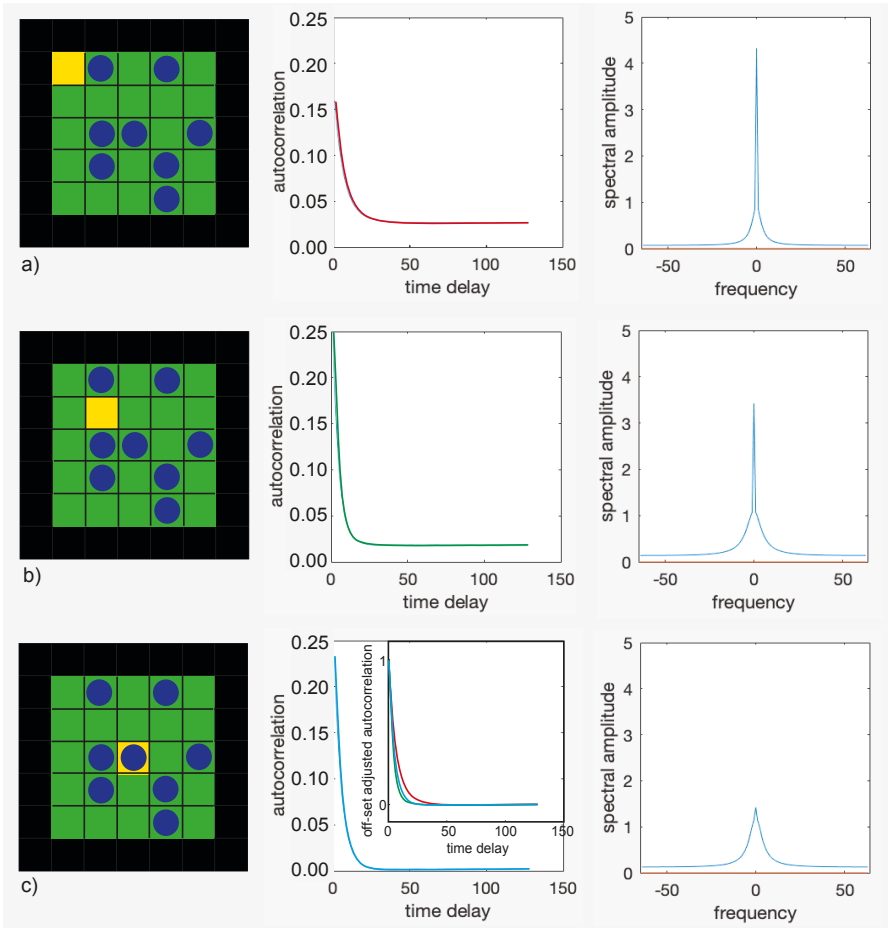

Figure 5. Autocorrelation functions (center) of the occupancy of the yellow cells (left) and the real parts of their Fourier transforms (right) for repulsive interaction at T = 0.1 and P = 0.3. a) Corner cell. b) Off-center cell. c) Center cell. The inset in the middle compares the decays of all three autocorrelation functions after subtraction of the offsets.

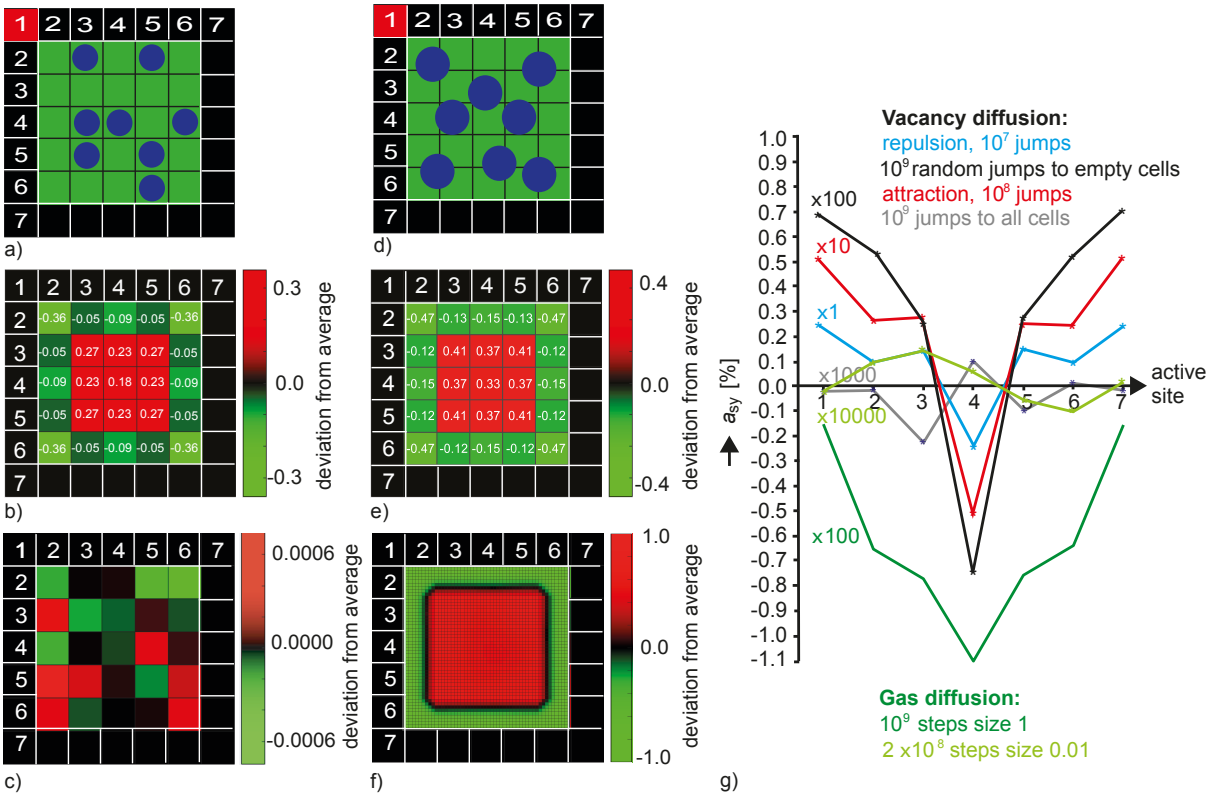

Figure 6. Population density distributions and dependences of the asymmetry parameter a_{sy} on the position of the active relaxation site in the wall of a pore with 5 × 5 cells. a) Vacancy diffusion. Particles can jump one step on the grid in 8 directions. b) Deviations from average relative density 1 for 10^9 jumps chosen at random to any of the free neighbor cells. c) Deviations from average relative density 1 for 10^9 jumps chosen at random to any of the 8 neighbor cells. d) Gas diffusion. The particle motion is computed on a fine grid. e) Deviations from average relative density 1 for 10^9 observations of particle positions at observation intervals of duration 1. The particle position at the time of observation is binned to the course vacancy-diffusion grid. f) Deviations from average relative density 1 on a fine 50×50 grid of 0.1 particle diameters for 10^9 observations of particle positions at observation intervals of duration 0.01. g) Variations of the asymmetry parameter with the position of the active site in the cell wall for differently interacting particles for vacancy diffusion at T = 0.2, P = 0.3, and different jump probabilities as well as for gas diffusion at long and short observation intervals of 1 vs. 0.01. The mirror symmetry of each trace about the center position reports high precision of the simulation.

While the autocorrelation function is difficult to probe experimentally, the asymmetry parameter a_{sy}, on the other hand, probes the particle dynamics and could be investigated experimentally directly by relaxation-exchange NMR experiments provided the signal-to-noise ratio is good enough. The parameter depends on the location of the relaxation center in the pore wall (Fig. 6). This dependence has been verified to be identical for all walls of the square pore. Moreover, it exhibits mirror symmetry about the center position (Fig. 6g), assuring that the simulation noise is negligible. For vacancy diffusion in a 5 × 5 square pore with walls 7 cells wide (Fig.

6a,b), a_{sy} varies consistently with position when the jumps are selected following *a priori* defined probabilities, irrespective of the particle interaction being positive, negative, or the destination cell having been chosen randomly from all free neighbor cells. But the magnitude of a_{sy} depends strongly on the selection rule defined by the jump probability as indicated in Fig. 6g by the scaling factors. It is highest at the corner positions and lowest at the center position. For random jumps to empty cells, a_{sy} is more than an order of magnitude smaller than for repulsive interaction, so that the number of particle jumps had to be increased to 10^9 resulting in 3 h computation time for each data point in the corresponding trace (black) Fig. 6e. Interestingly, for gas diffusion (Fig. 6d) a_{sy} varies at long observation interval (green, Fig. 6g) in a fashion similar to that for vacancy diffusion, is of magnitude comparable to that of vacancy diffusion (black, Fig, 6g), but does not change sign with position of the active site in the pore wall. In all these cases the precision of the asymmetry parameter a_{sy} obtained in the simulations exceeds the second relevant digit. If the jumps in the vacancy diffusion simulations are chosen without bias from a jump probability no exchange asymmetry is detected, only noise nearly more than one order of magnitude lower than for jumps selected at random to one of the free neighbor positions (grey, Fig. 6g). Similarly, the asymmetry parameter decreases with the observation time becoming shorter by more than two orders of magnitude as illustrated in Fig. 6g for a long time step of 1 (dark green) versus a short time step of 0.01 (light green) in simulation units of $(\mathrm{m\ s}^2 / k_{\mathrm{B}} T)^{1/2}$.

The particle dynamics manifested in a_{sy} are accompanied by variations of the average population density across the pore which is depleted in the contact layer of the particle with the pore wall, enhanced in the next layer, and tapers off towards the pore center in both cases (Figs. 6b,e, Fig. S4). The densities vary in a similar fashion across the pore for both types of diffusion albeit having somewhat different values as can be verified by close inspection of the numbers in each cell in Figs. 6b,e. These density variations disagree with Boltzmann's argument, that elastic collisions with the walls effectively remove the impact of the walls to the effect, that the walls can be neglected. Agreement, however, is reached, if the destination cells for particle jumps in vacancy diffusion are chosen at random from all and not just the free neighbor cells (Fig. 6c; Metropolis et al., 1953). Shortening the observation interval in the gas-diffusion simulations, however, maintains the unphysical density distribution across the pore and has no effect due to binning the particle positions to the vacancy-diffusion

grid at the time of observation, as the exact moment of a particle collision cannot be determined on a discrete time axis. On a finer grid, however, the population density is homogeneous except for the regions close to the walls, which the center of the circular particles cannot approach (Fig. 6f). If, however, projected onto the course vacancy-diffusion grid the population-density modulations (Fig. 6e) reappear, because the exact locations of collisions cannot be determined in a simple way at finite observation-time intervals. Nevertheless, for both algorithms, the asymmetry parameter approaches zero for all positions along the wall of the square pore (Fig. 6g, light green), confirming that detailed balance is observed.

The maps in Fig. 6b,c,e,f revealing the deviation of local population density from average population density were calculated by summing the 2D maps of particle locations after each jump or at each observation time, normalizing the resultant maps to the number of jumps and the particle density and subtracting the average mean expected for a constant particle density across all cells in the pore. Further maps of population density variations for the two different pores of Fig. 3 with other sizes and interaction parameters are summarized in Fig. S4 of the supplement. While the particle density varies less with temperature for vacancy diffusion, different density patterns are found at different pressures. The strongest density variations are near the pore wall whether the interaction is repulsive, attractive, or based on prior knowledge that a neighbor cell is occupied. This becomes particularly evident for larger pores (Figs. S4b,d,e). Coincidentally, at low density the main features of the density maps are strikingly similar for vacancy diffusion with destination cells chosen randomly from among the free neighbor cells (Figs. S4b) and gas diffusion (Figs. S4d). The particle density is strongly depleted at the pore corners and near the wall and significantly increased in the next particle layer (Figs. S4e,f). For interacting particles, this concentration variation is carried forward in vacancy diffusion with increasing distance from the wall leading to concentration waves which taper off towards the center of the pore and interfere with each other coming from different directions. For small pores interference patterns dominate the density distribution across the pore (Figs. 6b,e and Figs. S4a,c). For particles jumping randomly to empty neighbor cells, the decay of the concentration wave towards the pore center is fast with few to no oscillations towards the pore center, while the oscillations are enhanced by conditioning the jump probability with a hypothetical free jump energy (Fig. S4d, $P = 0.2$). In particular, the

population density at the active site in the dent of the complex pore of Fig. 3a depends on the parameters P and T (Figs. S4a,b).

4. Discussion

Confined two-dimensional diffusion has been modelled by two different algorithms to investigate in how far the cross-peaks in 2D T_2-T_2 exchange maps can be asymmetric. The asymmetry is quantified by an asymmetry parameter a_{sy} which reports the relative flux between two sites corresponding to the difference in the number of forward and backward exchanges normalized to the total number of exchanges. The vacancy-diffusion algorithm models particle jumps on a checkerboard grid to nearest neighbor cells under the constraint of different jump probabilities and samples the population map after each jump. The jump probability was determined from a Boltzmann distribution with a heuristic free energy which depends on the populations of the surrounding cells. The asymmetry parameters turned out to be equal to zero in the case of equal jump probability to all neighbor cells (Metropolis et al., 1953), whether occupied or not, confirming the validity of detailed balance (Fig. 6g). It was found to be different from zero when different jump probabilities were assigned to different neighbor cells, i. e. when the jump energy depended on the population pattern of the neighbor cells. But with the statistical arrangement of the particles on a checkerboard and the confinement of the interaction force to next nearest neighbors, energy is not conserved with a particle move, so that each particle move either injects or extracts energy from the system. Nevertheless, the equilibrium condition (3) is fulfilled, so that the system is not in thermodynamical equilibrium but rather in an equilibrium that is driven by the algorithm. The observed asymmetry parameter is, therefore, assigned to a driven and not thermodynamic equilibrium.

The gas-diffusion algorithm models particles colliding with initial velocity vectors and calculates new velocity vectors after a collision from conservation of energy and momentum, whereby the instant of a collision is interrogated on a discrete time grid. The smaller the observation time, the more precise the instant of a collision is determined. Any deviation from the exact collision time leads to errors in the position coordinates of the colliding particles and thus their velocities (Eqns. 7,8; Michel et al. 2014). While for large observation time a significant asymmetry parameter is observed (Fig. 6g, dark green) its value shrinks drastically when the observation time is reduced by a factor of 100 (Fig. 6g, light green). It is concluded that in the limit of infinitely short

observation time, also the gas-diffusion algorithm can produce vanishing asymmetry parameter in three-site exchange in agreement with the principle of detailed balance and with symmetry in the cross-peak intensities of exchange maps in thermodynamic equilibtium. If, on the other hand, the velocities are calculated with a systematic error in the gas-diffusion model due to a finite observation interval, the resultant velocities disagree with the energy and momenta of elastic collisions, so that also here energy is injected or extracted from the system and the observed asymmetry parameter can be attributed to a driven and not a thermodynamic equilibrium.

The asymmetry parameters observed for either of the two pore shapes (Fig. 3) investigated with the vacancy-diffusion model vary in a range on the order of $-1\% < a_{\mathrm{sy}} < 1\%$, i. e., up to 1% of all particles in the pore do not follow detailed balance between all pairs of sites but move coherently in circles between the three sites. It is emphasized that this circular exchange is between the pools of particles representing the three sites, and it is not a motion followed by individual particles completing circular jumps. Given repulsive or attractive interaction in the vacancy diffusion model with heuristic temperature and pressure dependent jump probabilities, the variations of a_{sy} with temperature T appear rapid, reminiscent of phase transitions (Figs. 4a,b, Figs. S3a). The variations of a_{sy} with pressure corresponding to population density P are smooth (Figs. 4d,e, Figs. S3b). Either positive or negative values of a_{sy} are observed as T or P change. A sign change of a_{sy} reports a change in the sense of the circular exchange (cf. Fig. 1).

For a simple square pore, the asymmetry parameter varies with the position of the active site in the cell wall, exhibiting mirror symmetry with respect to the wall center (Fig. 6g). The variation is the same for the different jump probabilities, referred to as repulsive and attractive interaction or random jumps to empty cells albeit it differs significantly in magnitude. A similar dependence is observed in the gas-phase diffusion simulations at long observation time. Moreover, the autocorrelations functions and their Fourier transforms have been determined for the occupancy time tracks of selected cells at specific positions inside a small square pore for 10^7 jumps of all particles in the pore (Fig. 5). The time-track function had been devised to have zero mean for the average cell population. Depending on the position of the cell inside the pore, the autocorrelations functions and their Fourier transforms vary. Specifically, the autocorrelation function can exhibit a significant constant offset. At these positions inside the pore, the particle densities are different from the pore average, and the cell

is on average emptier or more occupied than expected if the exchange between all cells were the same. This conclusion is supported by the observed deviations of the cell occupancies from the pore average (Figs. 6b,e, Fig. S4). Near the pore wall the average population density is depleted and varies in an oscillatory manner along the pore wall. Further towards the center of the pore the average population density increases sharply and then tapers off towards the pore center to a value slightly above the average density.

These observations for driven vacancy diffusion in a square pore with 5 × 5 cells are compared to independent simulations of driven gas diffusion (long observation time: step size 1) of non-interacting particles in a square pore with an edge length of 5 particle diameters also allowing 7 relaxation centers along the pore wall (Figs. 6a,d). A similar variation of the asymmetry parameter is found as for vacancy diffusion, but the asymmetry parameter is negative for all positions of the active site (Fig. 6g, dark green). Moreover, the depletion of the average particle density at the pore wall and its subsequent variation towards the center are similar with the exception, that oscillations of the average particle density along the pore wall are weaker for gas diffusion for the (Figs. 6b,e). These oscillations persist even at short observation times due to the uncertainty of localizing the particle positions at the exact time of their collision on a discrete time grid. The lack of a sign change in the asymmetry parameter with changing position of the active site may be explained by destructive interference of particle collisions from multiple sites with the wall within one discrete particle diameter and the fact, that the free path length between collisions in gas diffusion is not limited to the next cell as in vacancy diffusion but can range up to the pore diameter. Taken together, the observed asymmetry in the three-site exchange in driven equilibrium and the variation of the jump statistics with position inside the pore point at diffusive resonance phenomena like standing waves of air in pipes as reported by Kundt (Kundt, 1866) or of vibrating plates as reported by Chladni (Chladni, 1787).

Three-site exchange can be viewed as a finite difference approximation to the Laplace operator (van Kampen, 1992; Kuprov, 2022) governing Fick's second law (Fick, 1855). Considering some local site *N* with neighbor sites *N*-1 and *N*+1 right and left, the mass flow to and from site *N* given by Eqn. (1) is

$$\frac{\mathrm{d}m_N(t)}{\mathrm{d}t} = k_{N,N-1}m_{N-1} - k_{N-1,N}m_N + k_{N,N+1}m_{N+1} - k_{N+1,N}m_N, \tag{10}$$

Taking the limit to infinitesimal small distance $\Delta r \to \mathrm{d}r$ between the neighboring sites leads to $k_{j,i} = k$, revealing that (10) is a finite difference approximation of a second spatial derivative balanced by the temporal variations of m during infinitesimal time $\mathrm{d}t$,

$$(k\, m_{N-1} - 2\, k\, m_N + k\, m_{N+1})/\Delta r^2 \approx k \frac{\mathrm{d}^2 m}{\mathrm{d}r^2} = \frac{\mathrm{d}m}{\mathrm{d}t}/\Delta r^2. \tag{11}$$

In this limit, Eqn. (11) becomes Fick's second law with the diffusion coefficient $D = k\Delta r^2$. This back-of-the-envelope argument suggests that the observed asymmetry of three-site exchange is a property of Fick's second law and relates to igenmodes of the Laplace operator (Hoop and Prange 2007, Grebenkov and Nguyen 2013).

The diffusion equation applicable to longitudinal magnetization in NMR instead of particle masses m is the Bloch-Torrey equation (Torrey, 1956),

$$\frac{\partial}{\partial t} m(\boldsymbol{r}, t) = D \boldsymbol{\nabla}^2 m(\boldsymbol{r}, t) - \mu\, m(\boldsymbol{r}, t), \tag{12}$$

where m now is the magnetization deviation from thermal equilibrium and μ is the bulk relaxation rate. $m(\boldsymbol{r}, t)$ solves this equation in terms of an expansion into normalized eigenfunctions $\phi_n(\boldsymbol{r})$ with amplitudes A_n and eigenvalues τ_n (Brownstein and Tarr, 1977; Song, 2000)

$$m(\boldsymbol{r}, t) = e^{-\mu t} \sum_{n=0}^{\infty} A_n\, \phi_n(\boldsymbol{r})\, e^{-\frac{t}{\tau_n}}. \tag{13}$$

The eigenvalues are determined by the boundary condition

$$D\, \boldsymbol{n}\, \boldsymbol{\nabla} \phi_n(\boldsymbol{r}) = \rho\, \phi_n(\boldsymbol{r}), \tag{14}$$

where ρ is the surface relaxivity and $\boldsymbol{n}$ is the unit vector normal to the surface. They depend on the diffusion coefficient and determine the NMR relaxation time in different ways according to the pore geometry. The population ϕ_0 of the lowest normal mode has no nodes. The higher normal modes ϕ_n possess nodal surfaces. The higher diffusion eigenmodes have been detected by NMR with selective excitation of partial pore volumes making use of field gradients internal to the pore (Song, 2000). These experimental results reported by Song agree with the Monte Carlo simulations of driven diffusive translational motion in pores reported here, in that the population density varies across the pore and that the offset of the autocorrelation function of the local pore occupancy depends on the position of the cell in the pore. It needs to be investigated further how much the NMR relaxation times and the associated particle dynamics vary with the position from the pore wall to the center in the driven concentration wave (Bytchenkoff and Rodts, 2011). On the other hand, stochastic resonance in thermodynamic equilibrium has been observed with NMR first by Sleator, Hahn et al. (Sleator et al., 1985) and subsequently studied in detail by Müller,

Jerschow, et al. in different scenarios (Müller and Jerschow, 2005; Schlagnitweit and Müller, 2012). There, the magnetization fluctuating with the thermal motion of the nuclear spins assumes the role of the particles and the resonance circuit assumes the role of the pore. Diffusion eigenmodes are expected to be unobservable with this method unless a subset of modes is driven by an external stimulus, because they may be silent in thermodynamic equilibrium.

From the exchange asymmetry of the particles in the square pore investigated in Fig. 6 a suggestive picture emerges for driven confined vacancy diffusion (Fig. 7), where the diffusion lengths are confined to the distances from the particle to the direct neighbor cells. Depending on the sign of the asymmetry parameter (Fig. 7a), a small fraction of the particles (blue circles) prefers the direct path towards or away from the active site (red square) at the pore boundary over the path along the boundary to or from the active site. In the center of the wall, the direct path away from the active site to the bulk is preferred over the path along the pore wall when leaving the contact region with the active site (Fig. 7b). But because jumps are allowed in vacancy diffusion only to neighboring cells, the cells belonging to relaxation pool 2 at the wall right and left of the active site 3 must be populated from the bulk 1 by direct jumps form the bulk to the wall. For these jumps, the asymmetry parameter is indeed positive, as observed for the off-center positions of the active site (Fig. 6g). Given the symmetry of the square pore, the in-plane translational diffusion paths resulting from the variation of the asymmetry parameters with the position of the active site on the pore wall demand the existence of eight diffusion vortices inside the planar pore (Fig. 7d). The symmetry of this in-plane translational diffusion pattern matches the symmetry of one of the node patterns of the out-of-plane vibrational modes of a square plate observed by Chladni (Fig. 7e) about a quarter of a millennium earlier (Chladni, 1787). This also suggests that the dynamic of driven vacancy diffusion observed in the computer model reported here is a resonance feature of the pore and thus relates to diffusion eigenmodes. The resonance effect is less pronounced for gas diffusion (Fig. 7c) where the free paths between collisions can span the entire cell. Because the mass flow from relaxation site 2 to the active site 3 can be sustained from any position at the pore wall the asymmetry parameter does not need to change sign when the active site moves along the pore wall (Fig. 7e), and the circular paths can have various shapes and can extend across the entire pore, so that the vortex pattern is largely washed out.

Given the technological importance of fluid motion in small pores in heterogeneous catalysis (Kärger et al., 2012), it will be interesting to explore, if such correlated motion resulting from standing longitudinal particle-concentration wave patterns near pore walls can be driven by external stimuli like ultrasound, electric or magnetic fields. The standing waves could be enhanced by tuning the driver frequency to the pore resonance like a musician enforces resonance modes on a flute when playing. To enhance the resonance modes, also low-power broad-band, forced oscillations can be considered such as in Fourier transform infrared spectroscopy (Michelson, 1903) and stochastic NMR spectroscopy (Ernst, 1970), while triggering free oscillations by high-power impulses may destroy the porous medium under study.

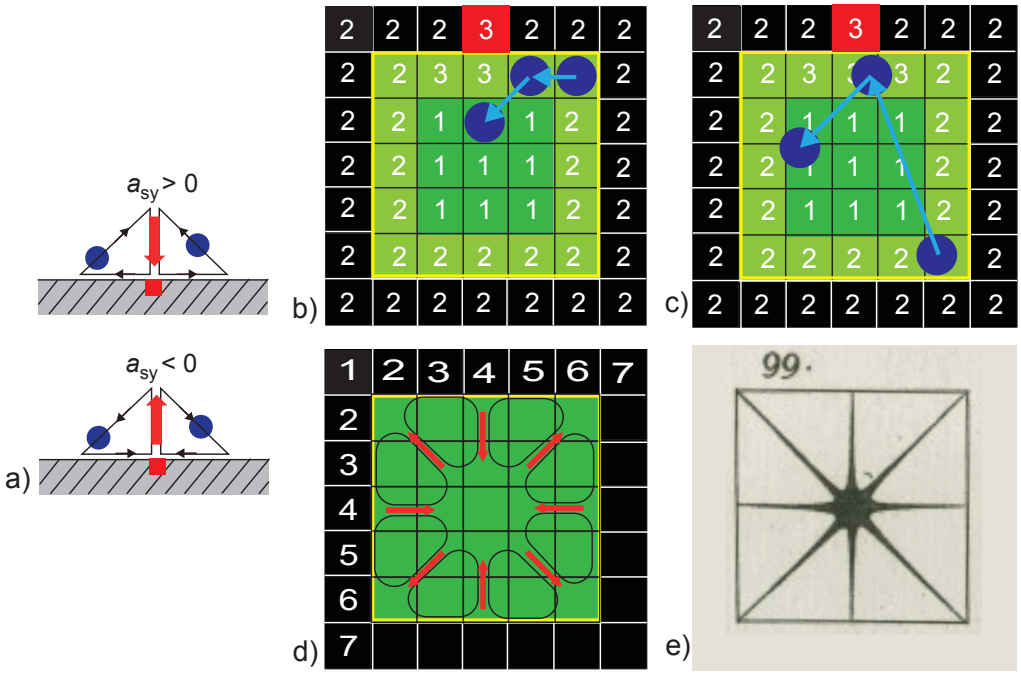

Figure 7. Illustration of the exchange asymmetry in driven equilibrium for the square pore of Fig. 6a. a) Depending on the sign of the asymmetry parameter, a small fraction of diffusing particles (blue circles) prefers the direct path towards or away from the active site (red square) at the pore boundary over the path along the boundary from the active site. b) Vacancy diffusion for negative asymmetry parameter and the active site 3 in the center of the pore wall. Jumps are limited to the next nearest cells. The direct path away from the active site to the bulk 1 in the center is preferred over the path along the pore wall 2 when leaving the contact region with the active site. c) Gas diffusion for negative asymmetry parameter and the active site 3 in the center of the pore wall. The free paths between collisions can span the entire cell. d) In-plane translational vacancy-diffusion paths resulting from the variation of the asymmetry parameters with the position of the active site on the pore wall depicted in Fig. 6g. e) Out-of-plane vibrational mode of a square plate observed by Chladni (Chladni, 1787).

5. Summary

The evidence provided by Monte Carlo simulations of random particle jumps on a 2D checkerboard and by simulations of 2D gas diffusion with topological confinements supports the notion, that asymmetry in three-site exchange maps reports the non-Brownian diffusion dynamics of confined particles in driven equilibrium. Depending on the sign of the asymmetry parameter, a small fraction of all particles prefers the direct path towards or away from the active site at the pore boundary over the path along the boundary to or from the active site resulting in a circular flux (Fig. 7). Both, driven vacancy diffusion and driven gas diffusion produce congruent results. These are: 1) Circular exchange is a manifestation of driven equilibrium and leads to asymmetry of exchange peaks, while thermodynamic equilibrium manifests itself in detailed balance and symmetry of exchange peaks. 2) The circular exchange in driven equilibrium appears to be a resonance phenomenon which can potentially be driven by external stimuli. Yet, the reported simulations are limited to two dimensions, and it may be argued that the asymmetry of exchange vanishes in the more common pores with three spatial dimensions. But two-dimensional diffusion is not an abstract model and arises for gas atoms adsorbed to metal surfaces (Oura et al., 2013), so that the driven coherent particle diffusion indicated by the non-zero asymmetry parameter may be observed there. Given the congruent simulation evidence for driven vacancy diffusion and gas diffusion in two-dimensional confinements it is hypothesized, that confined diffusion can be partially converted to coherent motion by external excitation so that detailed balance will be violated as observed in nonequilibrium phenomena (Gnesotto et al. 2018, Lynn et al. 2021).

Author Contributions

BB posed the question, executed the simulations of confined vacancy diffusion, and wrote the manuscript. MA worked out the algorithm for vacancy diffusion along with BB and supervised MP. MP programmed the algorithm for confined gas diffusion and executed the gas-diffusion simulations.

Acknowledgement

BB thanks Thomas Wiegand at RWTH Aachen University for stimulating discussions, hosting him as a PostProf, and access to the computing facilities. He also thanks Ilya Kuprov for his flash of inspiration on linking three-site exchange to Fick’s second law

at a random EUROMAR 2022 breakfast encounter and Stephan Appelt, Gerd Buntkowsky, Jeffrey Reimer, and Tom Barbara for stimulating discussions. Special thanks go to the unknown reviewer who commented on the manuscript (Gao and Blümich, 2020), that asymmetry in three-site exchange violates the principle of detailed balance and to the anonymous reviewer of this manuscript who educated the authors on the intricacies of Monte Carlo simulations.

Code availability

The codes for simulating confined 2D vacancy diffusion and confined 2D gas diffusion are reported in the supplement.

Conflict of Interest statement

Other than that BB is on the advisory board of Magnetic Resonance the authors declare no conflict of interest.

References

Bialynicki-Birula, I. and Bailynicky-Birula, I., Modeling Reality, Oxford University Press, Oxford, 2004.

Björgvinsdóttir, S., Moutzouri, P., Walder, B. J., Matthey, N., and Emsley, L., Hyperpolarization transfer pathways in inorganic materials, J. Magn. Reson. 323, 106888, 2021.

Brownstein, K.R. and Tarr, C. E., Spin-Lattice Relaxation in a System Governed by Diffusion, J. Magn. Reson. 26, 17–24, 1977.

Bunde, A., Caro, J., Kärger, J., and G. Vogel, eds., Diffusive Spreading in Nature and Technology, Springer Nature, Cham, 2018.

Bytchenkoff, D., and Rodts, S., Structure of the two-dimensional relaxation spectra seen within the eigenmode perturbation theory and the two-site exchange model, J. Magn. Reson. 208, 4–19, 2011.

Callaghan, P. T. and Stepišnik, J., Modulated Gradient NMR, J. Magn. Reson. 117, 118–122 (1995).

Callaghan, P.T., Translational Dynamics and Magnetic Resonance: Principles of Pulsed Gradient Spin Echo NMR, Oxford University Press, Oxford, 2011.

Chladni, E. F. F., Entdeckungen über die Theorie des Klanges, Leipzig, Weidmanns Erben und Reich, 1787.

de Hoop, A.T. and Prange, M.D., Variational analysis of the natural decay rates and eigenmodes of cavity-enclosed diffusive fields, J. Phys. A: Math. Theor. 40, 12463–12477, 2007.

Einstein, A., Zur Quantentheorie der Strahlung, Physikalische Zeitschrift 18, 121–128, 1917.

Ernst, R. R., Bodenhausen, G., and Wokaun, A., Principles of Nuclear Magnetic Resonance in One and Two Dimensions, ClarendonPress, Oxford, 1987.

Ernst, R. R., Magnetic Resonance with Stochastic Excitation, J. Magn. Res. 3, 10–27, 1970.

Feynman, R., Leighton, R. B., and Sands, M., The Feynman Lectures on Physics, vol. 1, chapter 46, Addison-Wesley, Reading, Fourth Printing, 1966

Fick, A., Ueber Diffusion, Annalen der Physik 94, 59–86, 1855.

Gao, Y., and Blümich, B., Analysis of three-site T_2-T_2 exchange NMR, J. Magn. Reson. 315, 106740, 2020.

Gnesotto, F. S., Mura, F., Gladrow, J., and Broedersz, C. P., Broken detailed balance and non-equilibrium dynamics in living systems: a review, Rep. Prog. Phys. 81, 066601, 2018.

Grebenkov, D. S., A fast random walk algorithm for computing the pulsed-gradient spin-echo signal in multiscale porous media, J. Magn. Reson. 208, 243–255, 2011.

Grebenkov, D. S. and Nguyen, B.-T., Geometrical Structure of Laplacian Eigenfunctions, SIAM Review 55, 601–667, 2013.

Han, S.-I. and Blümich, B., Two-dimensional representation of position, velocity, and acceleration by PFG-NMR, Appl. Magn. Res. 18, 101–114, 2000.

Hughes, B. D., Random Walks and Random Environments, Clarendon Press, Oxford, 1995.

Jeener, J., Meier, B. H., Bachmann, P., and Ernst, R. R., Investigation of exchange processes by two-dimensional NMR spectroscopy, J. Chem. Phys. 71 4546–4553, 1979.

Kärger, J., Ruthven, D. M., and Theodorou, D. N., eds., Diffusion in Nanoporous Materials, vol. 1, Wiley-VCH, Weinheim, 2012.

Kundt, A., Über eine neue Art akustischer Staubfiguren und über die Anwendung derselben zur Bestimmung der Schallgeschwindigkeit in festen Körpern und Gasen, Annal. Phys. Chem. 203, 497–523, 1866.

Kuprov, I., private communication with BB at the EUROMAR 2022 conference in Utrecht, July 10–14, 2022.

Boltzmann, L., Weitere Studien über das Wärmegleichgewicht unter Gasmolekülen, Sitzungsber. Kais. Akad. Wiss., Wien, Math, Natruwiss. Classe 66, 275-370, 1872.

Lacabanne, D., Wiegand, T., Di Cesare, M., Orelle, C., Ernst, M., Jault, J.-M., Meier, B.H., and Böckmann, A., Solid-State NMR Reveals Asymmetric ATP Hydrolysis in the Multidrug ABC Transporter BmrA, J. Am. Chem. Soc. 144, 12431–12442, 2022.

Lee, J.-H., Labadie, C., Springer Jr., C. S., and Harbison G.S., Two-Dimensional Inverse Laplace Transform NMR: Altered Relaxation Times Allow Detection of Exchange Correlation, J. Am. Chem. Soc. 115, 7761–7764, 1993.

Lynn, C. W., Cornblath, W. J., Papadopoulos, L., Bertolerod, M. A., and Bassett, D. S., Broken detailed balance and entropy production in the human brain, PNAS 118, e2109889118, 2021.

Maxwell, J. C., On the dynamical theory of gases, Philos. Trans. R. Soc. London 157 49–88, 1867.

McDonald, P. J., Korb, J.-P., Mitchell, J., and Monteilhet, L., Surface relaxation and chemical exchange in hydrating cement pastes: A two-dimensional NMR relaxation study, Phys. Rev. E 72, 011409, 2005.

Metropolis, N., Rosenbluth, A.W., Rosenbluth, M.N., Teller, A.H., and Teller, E., Equation of State Calculations by Fast Computing Machines, J. Chem. Phys. 21, 1087–1092, 1953.

Michel, M., Kapfer S. C., and Krauth, W., Generalized event-chain Monte-Carlo: Constructing rejection-free global-balance algorithms from infinitesimal steps, J. Chem. Phys. 140 054116, 2014.

Michelson, A. A., Light Waves and Their Uses, The University of Chicago Press, Chicago, 1903.

Müller, N. and Jerschow, A., Nuclear Spin Noise Imaging, PNAS 103, 6790–6792, 2005.

Olaru, A. M., Kowalski, J., Sethi, V., and Blümich, B., Exchange relaxometry of flow at small Péclet numbers in a glass bead pack, J. Magn. Reson. 220, 32–44, 2012.

Onsager, L., Reciprocal Relations in Irreversible Processes, Phys. Rev. 37, 405-426, 1931.

Oura, K., Lifshits, V. G., Saranin, A. A., Zotov, A. V., and Katayama, M., Surface Science: An Introduction, Springer, Berlin, 2013, chapter 13.

Parsons, E. C., Does, M. D., and Gore J.C., Temporal Diffusion Spectroscopy: Theory and Implementation in Restricted Systems Using Oscillating Gradients, Magn. Reson. Med. 55, 75–84, 2006.

Reviewer 2023, anonymous reviewer of Blümich, B., Parziale, M., and Augustine, M., Monte-Carlo Analysis of Asymmetry in Three-Site Relaxation Exchange: Probing Detailed Balance, Magnetic Resonance Preprint, 2023, doi.org/10.5194/mr-2023-8.

Sabelfeld, K. K., Monte Carlo Methods in Boundary Value Problems, Springer-Verlag, Berlin, 1991.

Sandstrom, J., Dynamic NMR Spectroscopy, Academic Press, Cambridge, MA, 1983

Schlagnitweit, J. and Müller, N., The first observation of Carbon-13 spin noise spectra, J. Magn. Reson. 224, 78–81, 2012.

Seitz, F., On the Theory of Vacancy Diffusion in Alloys, Phys. Rev. 74, 1513–1523, 1948.

Sleator, T., Hahn, E.L., Hilbert, C., and Clarke, J., Nuclear Spin Noise, Phys. Rev. Lett. 55, 1742–1745, 1985.

Song, Y. Q., Detection of the High Eigenmodes of Spin Diffusion in Porous Media, Phys. Rev. Lett 85, 3887–3881, 2000.

Song, Y.-Q., Venkataraman, L., Hürlimann, M. D., Flaum, M., Frulla, P., and Straley, C., T_1-T_2 Correlation Spectra Obtained by Using a Fast Two-Dimensional Laplace Inversion, J. Magn. Reson. 154, 261–268, 2002.

Stepišnik, J., Mohoric, A., Lahajnar, G., Mattea, C., Stapf, S., and Sersa, I., Velocity autocorrelation spectra in molten polymers measured by NMR modulated gradient spin-echo, Europhysics Lett. 106, 27007, 2014.

Torrey, H. C., Bloch Equations with Diffusion Terms, Phys. Rev. 104, 563–565, 1956.

Valiullin, R., ed., Diffusion NMR of Confined Systems, R. Soc. Chem., Cambridge, 2017.

van Kampen, N. G., Stochastic Processes in Physics and Chemistry, Elsevier, Amsterdam, 1992.

Van Landeghem, M., Haber, A., d'Espinose de Lacaillerie J.-B., and Blümich, B., Analysis of Multisite 2D Relaxation Exchange NMR, Concepts Magn. Reson. 36A, 153–169, 2010.

Wolf-Gladrow, D. A., Lattice-Gas Cellular Automata and Lattice Boltzmann Models, Springer, Berlin, 2000.